

Geometric signature of reversal modes in ferromagnetic nanowires

C. TANNOUS, A. GHADDAR AND J. GIERALTOWSKI

Laboratoire de Magnétisme de Bretagne - CNRS FRE 3117

Université de Bretagne Occidentale -

6, Avenue le Gorgeu C.S.93837 - 29238 Brest Cedex 3 - FRANCE

PACS. nn.mm.xx – 75.75.+a.

PACS. nn.mm.xx – 75.60.Ch.

PACS. nn.mm.xx – 75.75.+a.

PACS. nn.mm.xx – 75.60.Jk.

Abstract. – Magnetic nanowires are a good platform to study fundamental processes in Magnetism and have many attractive applications in recording such as perpendicular storage and in spintronics such as non-volatile magnetic memory devices (MRAM) and magnetic logic devices. In this work, nanowires are used to study magnetization reversal processes through a novel geometric approach. Reversal modes imprint a definite signature on a parametric curve representing the locus of the critical switching field. We show how the different modes affect the geometry of this curve depending on the nature of the anisotropy (uniaxial or cubic anisotropy), demagnetization and exchange effects. The samples we use are electrochemically grown Nickel and Cobalt nanowires.

Introduction. – A surge of renewed interest in ferromagnetic nanowires has occurred very recently triggered by their interesting properties with respect to spintronic devices and more specifically to non-volatile memory (MRAM) and logic devices [1–3].

From a fundamental point of view, they represent a quasi-one dimensional system displaying magnetic properties in sharp contrast to the Mermin-Wagner [4] theorem forbidding (Heisenberg-type) Magnetism in systems of dimension ($D \leq 2$) with short-range interactions.

They are simpler than nanotubes since their physical properties do not depend on chirality and they can be grown in a variety of methods: Molecular Beam Epitaxy, Electrochemical methods (Template synthesis, Anodic Alumina filters), Chemical solution techniques (Self-assembly, Sol-Gel, emulsions...) etc...

Template synthesis is an electrochemical method used in the manufacturing of nanostructured materials, in particular, nanowires can be obtained by filling a porous polycarbonate membrane, which contains a large number of cylindrical holes that are track-etched and possessing a narrow size distribution.

Individual nanowires as well as arrays of nanowires are important. Characterization and understanding of the magnetic properties of nanowire arrays are challenging since we have

dipolar interactions between wires in addition to anisotropy, magnetostatic and exchange effects within individual wires.

Many questions remain open regarding the detailed mechanisms responsible for the magnetization reversal. The intrinsic properties of nanowire arrays are directly related to the properties of the nanoporous template such as the relative pore orientations in the assembly, pore size and its distribution, as well as interpore distance.

Two reversal modes have been suggested as being important: curling and the coherent rotation depending on the value of the radius a with respect a cutoff value also called "coherence" radius R_{coh} .

For wire radius $a > R_{coh}$, the reversal occurs by curling. For $a < R_{coh}$, the coherent rotation is expected as predicted by the Stoner-Wohlfarth model [5].

The remanent magnetization distribution within a nanowire depends on its radius as well as on the balance between different contributions (anisotropy, magnetostatic/shape and exchange) to the magnetic energy. Exchange energy dominates at small wire radius and favors a uniform magnetization distribution or non-uniform flower, S, Landau, leaf... states. On the other hand, this almost collinear spin alignment leads to large demagnetizing fields due to magnetic surface charges and correspondingly increase of the magnetostatic energy which increases gradually with radius. When the radius increases beyond the single domain limit ($a > R_{sd}$), the competition between these two energies and anisotropy energy leads to non-uniform magnetic states such as multi-domain states (if the anisotropy constant is greater than the magnetostatic energy). It might lead to magnetic vortices, if the anisotropy energy is small in comparison with magnetostatic energy.

In this work, we set out to study the geometric signature of reversal modes in nanowires depending on the different magnetic properties inherent to the wire belonging to any of the anisotropy, magnetostatic and exchange classes. This paper is organised as follows: In section II, the geometric signature is discussed in the case of an infinite cylinder with a uniaxial anisotropy. In section III, the resulting parametric curve is considered for a general ellipsoid with arbitrary uniaxial anisotropy and finally section IV bears our conclusions.

Geometric signature of an infinite cylinder. – The geometric signature of a reversal mode is a parametric curve derived from the nanowire magnetization configuration that can be determined from the Brown equation by minimizing the total free energy [6].

In bulk ferromagnetic materials, the energy of the system can be minimized by forming multiple magnetic domains within which the magnetic moments are aligned. However, there is a critical size R_{sd} below which a particle remains in a single-domain state during switching; it is given by the implicit form:

$$R_{sd} = \sqrt{\frac{3A}{2\pi N_c M_s^2} \left[\ln\left(\frac{4R_{sd}}{a_0}\right) - 1 \right]} \quad (1)$$

derived by Frei *et al.* [7] after approximating the nanowire by an ellipsoid of revolution with major axis c and minor axis, $a = b \neq c$ and comparing the exchange energy averaged over the ellipsoid volume to the average magnetostatic energy (see Fig. 1).

For Nickel, the following parameters might be used: $M_s = 485 \text{ emu/cm}^3$, $a_0 = 0.249 \text{ nm}$ [8].

The curling reversal mode is the dominant magnetization reversal process in magnetic nanowires. The magnetization curling mode was defined by Frei *et al.* [7] and after it has used for different structure to investigate the magnetic switching of films, spherical particles, prolate ellipsoid and cylinders [9].

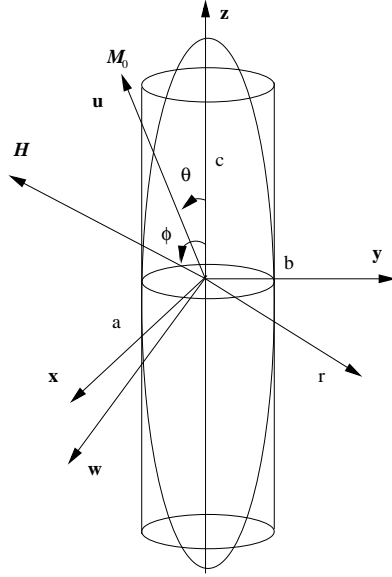


Fig. 1 – Cylindrical nanowire approximated by an ellipsoid of revolution of radius $a = b$ and long axis c . The nanowire is considered as a single domain with uniaxial anisotropy and in presence of applied field \mathbf{H} . The long axis of the ellipsoid taken along the z direction is also the anisotropy axis. The $(\mathbf{u}, \mathbf{v}, \mathbf{w})$ frame is such that the equilibrium magnetization \mathbf{M}_0 direction defines the \mathbf{u} axis. \mathbf{M}_0 lies in the (\mathbf{y}, \mathbf{z}) plane as well as the (\mathbf{u}, \mathbf{w}) basis obtained from it through rotation by the equilibrium angle θ (see Appendix).

The coherence radius R_{coh} separating uniform rotation and curling is given by:

$$R_{coh} = \frac{q}{M_s} \sqrt{\frac{A}{2\pi N_a}}, \quad (2)$$

A is the exchange stiffness ($A = 1.5 \times 10^{-6}$ erg/cm for bulk Nickel and Cobalt), M_s is the saturation magnetization and N_a is the demagnetization coefficient along the nanowire radius (see Fig. 1). The parameter q , is the smallest positive zero of the first kind Bessel function $J_1(x)$ derivative $\frac{dJ_1(x)}{dx}$ [10] (i.e. smallest positive maximum) and the smallest of the derivative of all ellipsoidal harmonics. It has been evaluated by Aharoni [11] to a 10^{-7} accuracy. He also found an accurate interpolation formula for any aspect ratio $m = c/a$:

$$q = \sum_{i=0}^5 \frac{b_i}{m^i} \quad (3)$$

with coefficients : $b_0 = 1.84120, b_1 = 0.48694, b_2 = -0.11381, b_3 = -0.50149, b_4 = 0.54072, b_5 = -0.17200$, that are accurate to 10^{-6} .

For particle size larger than R_{coh} yet smaller than R_{sd} , magnetization reversal proceeds through curling. In this mode, magnetization switching is an abrupt process, and the switching field is very close to the nucleation field for all angles.

In the case of an Infinite cylinder with a uniaxial anisotropy along the axis K , two distinct calculations were made independently by Chung and Muller [12] and Ishii [13] 20 years apart.

The curling equations (see Appendix) to be solved are:

$$\begin{aligned}\frac{H}{2\pi M_s} \sin(\theta - \phi) &= - \left[\frac{1}{4} + \frac{K}{4\pi M_s^2} \right] \sin 2\theta \\ \frac{H}{2\pi M_s} \cos(\theta - \phi) &= \frac{1}{2} \sin^2 \theta - \alpha - \frac{K}{4\pi M_s^2} \left[\frac{\cos 2\theta + \cos^4 \theta}{1 + \cos^2 \theta} \right]\end{aligned}\quad (4)$$

It is remarkable that the constant $\tilde{k} = \frac{7 \times 72}{11 \times 27 \times \pi}$ that appears in $\alpha = \frac{\tilde{k}}{S^2}$ is a rational approximation to the first zero of the Bessel function derivative $\frac{dJ_1(x)}{dx}$. This originates from the way Ishii [13] used the Bessel function in the average energy calculation (see Appendix and next section). The parameter S is the reduced radius defined as $S = a/\ell_{ex}$, with ℓ_{ex} the exchange length [14] considered as an intrinsic length scale of the nanowire (e.g. $\ell_{ex}=20.6$ nm for Nickel). $S = 0$ in coherent rotation (Stoner-Wohlfarth [5] limit), $S = 1$ in buckling whereas $S > 1$ in curling with the corresponding parametric curves displayed in Fig. 2.

The switching field components $h_x = \frac{H \sin(\phi)}{2\pi M_s}$, $h_z = \frac{H \cos(\phi)}{2\pi M_s}$ are then obtained as:

$$\begin{aligned}h_x &= \sin \theta \left[1 - \alpha + \frac{K \sin^2 \theta}{\pi M_s^2 (1 + \cos^2 \theta)} \right] \\ h_z &= -\cos \theta \left[\alpha + \frac{2K \sin^2 \theta}{\pi M_s^2 (1 + \cos^2 \theta)} \right]\end{aligned}\quad (5)$$

The above equations do not produce the coherent rotation limit as $S \rightarrow 0$ in which case, one writes:

$$\begin{aligned}h_x &= \left(\frac{K}{2\pi M_s^2} + 1 \right) \sin^3 \theta \\ h_z &= -\left(\frac{K}{2\pi M_s^2} + 1 \right) \cos^3 \theta\end{aligned}\quad (6)$$

There is a discrepancy in the results obtained by Ishii [13] and Chung and Muller [12] whose α and anisotropy K factors are off by a factor of $\frac{1}{2}$.

Geometric signature of a finite ellipsoid with arbitrary uniaxial anisotropy. – Let us consider the general case of an ellipsoid with fourth-order uniaxial anisotropy characterized by two constants K_1 and K_2 . Following Aharoni [9], Wegrowe *et al.* [17] performed a detailed study of Template synthesised Nickel nanowires and concluded that the anisotropy of their nanowires is positive and large (recall that for bulk Nickel, the lowest order *cubic* anisotropy constants [15] are $K_1 = -4.5 \times 10^4$ erg/cm³ and $K_2 = 2.3 \times 10^4$ erg/cm³ at room temperature) arguing that a large strain acting on the nanowires may induce such a large anisotropy change.

The curling equations to be solved in presence of fourth-order uniaxial anisotropy are:

$$\begin{aligned}\frac{H}{2\pi M_s} \sin(\theta - \phi) &= f(\theta) \\ \frac{H}{2\pi M_s} \cos(\theta - \phi) &= g(\theta)\end{aligned}\quad (7)$$

with the definitions:

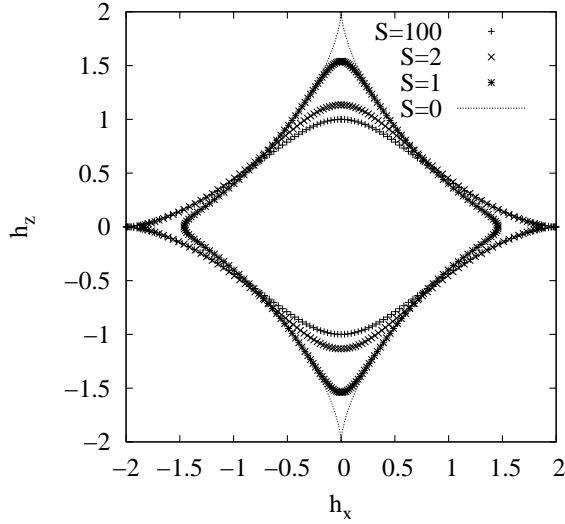


Fig. 2 – Parametric curve for an infinite cylinder with uniaxial anisotropy. We choose the normalised anisotropy constant $\frac{K}{2\pi M_s^2} = 0.5$ and several reduced radii $S = 1, 2$ and 100. The perfect Stoner-Wohlfarth astroid occurs when $S = 0$.

$$\begin{aligned}
 f(\theta) &= \left(N_a - N_c + \frac{K_1}{2\pi M_s^2} + \frac{K_2}{2\pi M_s^2} \sin^2 \theta \right) \sin 2\theta \\
 g(\theta) &= 2(N_a \sin^2 \theta + N_c \cos^2 \theta) - \alpha - \frac{K_1}{2\pi M_s^2} (3 \cos^2 \theta - 1) - 2 \frac{K_2}{2\pi M_s^2} (5 \cos^2 \theta - 1) \sin^2 \theta
 \end{aligned} \tag{8}$$

The parameter $\alpha = \frac{k}{S^2}$ with $k = \frac{q^2}{\pi}$ according to Aharoni’s [9] work, is a monotonically decreasing function of the aspect ratio of the ellipsoid like the parameter q (see Introduction). As an example, when $S = 2.06$ the Nickel nanowire radius is about 41.2 nm (see Figs. 3 and 4).

Aharoni’s approach is based on an isotropic approximation of the inhomogeneous components of the curling magnetization. Following Muller and Goldstein [16], we have developed a different set of curling equations in presence of fourth-order uniaxial that is free from the isotropic approximation as well as in presence of cubic anisotropy. In each case we get an appropriate $g(\theta)$ function as given below.

In our fourth-order uniaxial case [15], $g(\theta)$ is given by:

$$g(\theta) = 2(N_a \sin^2 \theta + N_c \cos^2 \theta) - \alpha - \frac{(K_1 + 2K_2)}{2\pi M_s^2} \cos 2\theta - 2 \frac{K_2}{2\pi M_s^2} \cos^2 \theta (3 \sin^2 \theta - \cos^2 \theta) \tag{9}$$

whereas in the sixth-order cubic anisotropy [15] case, it is given by:

$$g(\theta) = 2(N_a \sin^2 \theta + N_c \cos^2 \theta) - \alpha - \frac{K_1}{2\pi M_s^2} (1 - 5 \cos^2 \theta \sin^2 \theta) - \frac{K_2}{4\pi M_s^2} \sin^2 \theta \cos^2 \theta \tag{10}$$

Equations 8 (along with the different definitions of the $g(\theta)$ function) can be used to extract the components of the switching field h_x, h_z as before:

$$\begin{aligned}\phi &= \theta - \tan^{-1} \left[\frac{f(\theta)}{g(\theta)} \right] \\ h_x &= \sin(\theta)g(\theta) - \cos(\theta)f(\theta) \\ h_z &= \cos(\theta)g(\theta) + \sin(\theta)f(\theta)\end{aligned}\quad (11)$$

We use the same parameters as Wegrowe *et al.* [17], $K_1 = 2.0 \times 10^5 \text{ erg/cm}^3$, $K_2 = 0 \text{ erg/cm}^3$ and compare them to the Nickel bulk values at room temperature.

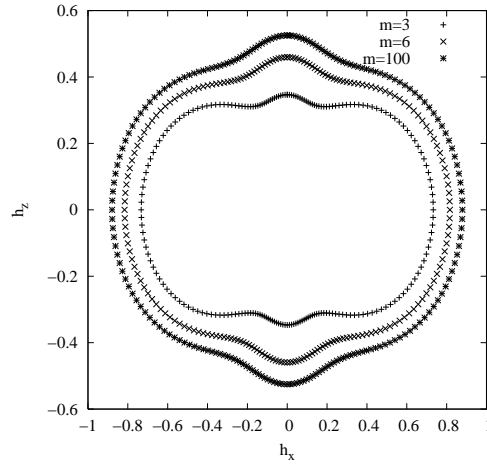


Fig. 3 – Geometric signature in the Wegrowe *et al.* case [17] ($K_1 = +2.0 \times 10^5 \text{ erg/cm}^3$ whereas $K_2 = 0. \text{ erg/cm}^3$) for three aspect ratios $m = c/a = 3, 6$ and 100 . The reduced radius in all cases is $S = 2.06$.

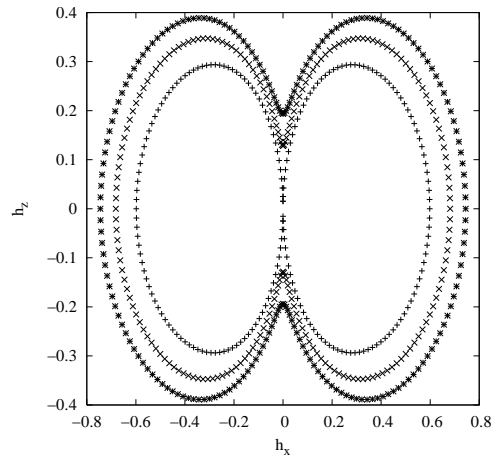


Fig. 4 – Geometric signature for bulk Ni at room temperature $K_1 = -4.5 \times 10^4 \text{ erg/cm}^3$, $K_2 = 2.3 \times 10^4 \text{ erg/cm}^3$) for three aspect ratios $m = c/a = 3, 6$ and 100 . The reduced radius is $S = 2.06$.

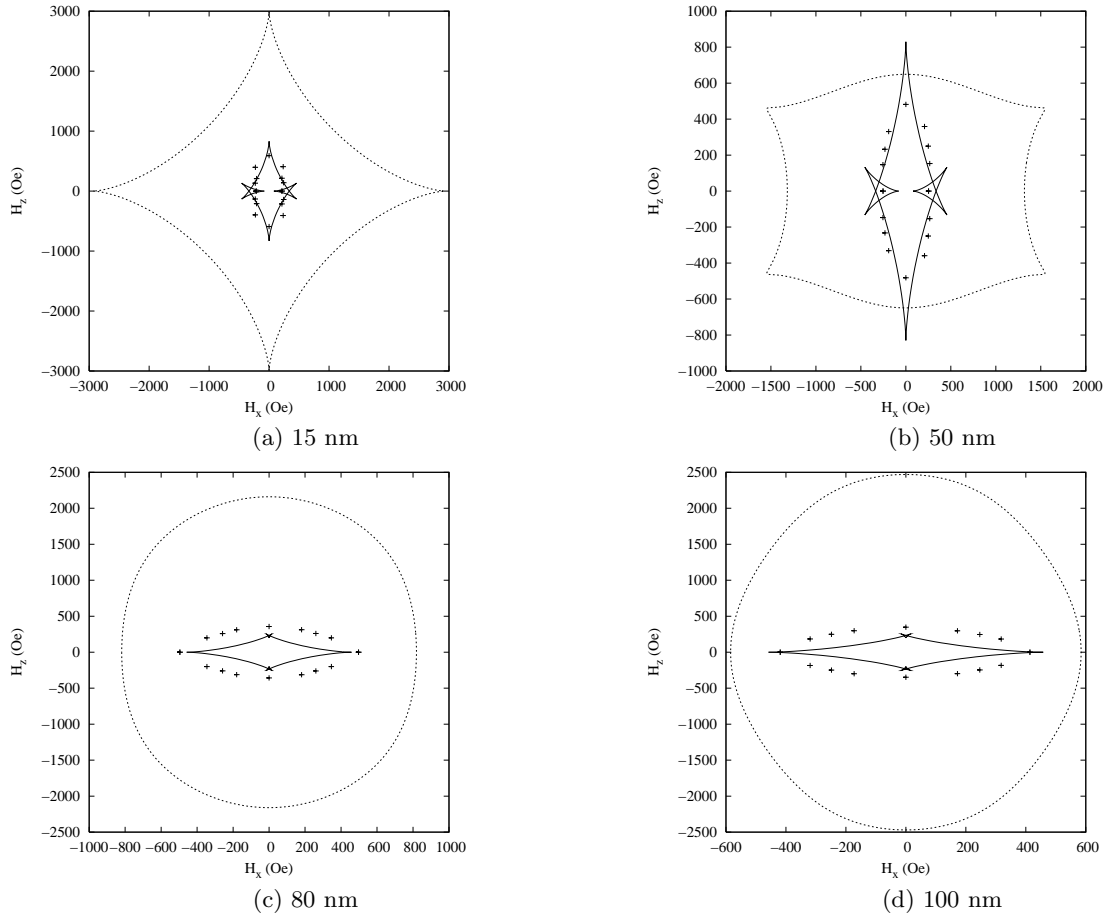


Fig. 5 – Comparison of least-squares fitting and measurements (+) on all Nickel nanowires in the uniaxial case. Geometric signature for the Ni nanowire experimental results with four sets of diameters: 15, 50, 80 and 100 nm. The fitting values are respectively: $M_s = 195 \text{ emu/cm}^3$, $K_1 = -223420 \text{ erg/cm}^3$ and $K_2 = 73198 \text{ erg/cm}^3$ for 15 and 50 nm and $M_s = 56 \text{ emu/cm}^3$, $K_1 = 6035 \text{ erg/cm}^3$ and $K_2 = -7255 \text{ erg/cm}^3$ for 80 and 100 nm diameters. The reduced radius is $S = 0.728, 2.427, 3.883$ and 4.854 respectively. The framing curves are obtained from the fitted K_1 , K_2 and the bulk value of M_s .

Our experimental results for the four diameter nanowires are fitted with a least-squares method to the fourth-order uniaxial case (in the Aharoni and our cases) as well as to the sixth order cubic anisotropy case and are displayed in Figs. 5 and 6 for Nickel and the same is done for Cobalt in the fourth-order uniaxial case only (see Fig. 7).

Recalling that for Nickel, the room temperature bulk values are: $M_s = 485 \text{ emu/cm}^3$, cubic [15] anisotropy constants: $K_1 = -4.5 \times 10^4 \text{ erg/cm}^3$, $K_2 = 2.3 \times 10^4 \text{ erg/cm}^3$ and for Cobalt, the room temperature bulk values are: $M_s = 1400 \text{ emu/cm}^3$, uniaxial [15] anisotropy constants $K_1 = -9 \times 10^5 \text{ erg/cm}^3$ and $K_2 = -2 \times 10^5 \text{ erg/cm}^3$, the least-squares fitting results show that the geometric approach to reversal modes (SW and curling) allows to have a good insight regarding the nature of the reversal modes despite the fact some of the fitting values depart substantially from the bulk values.

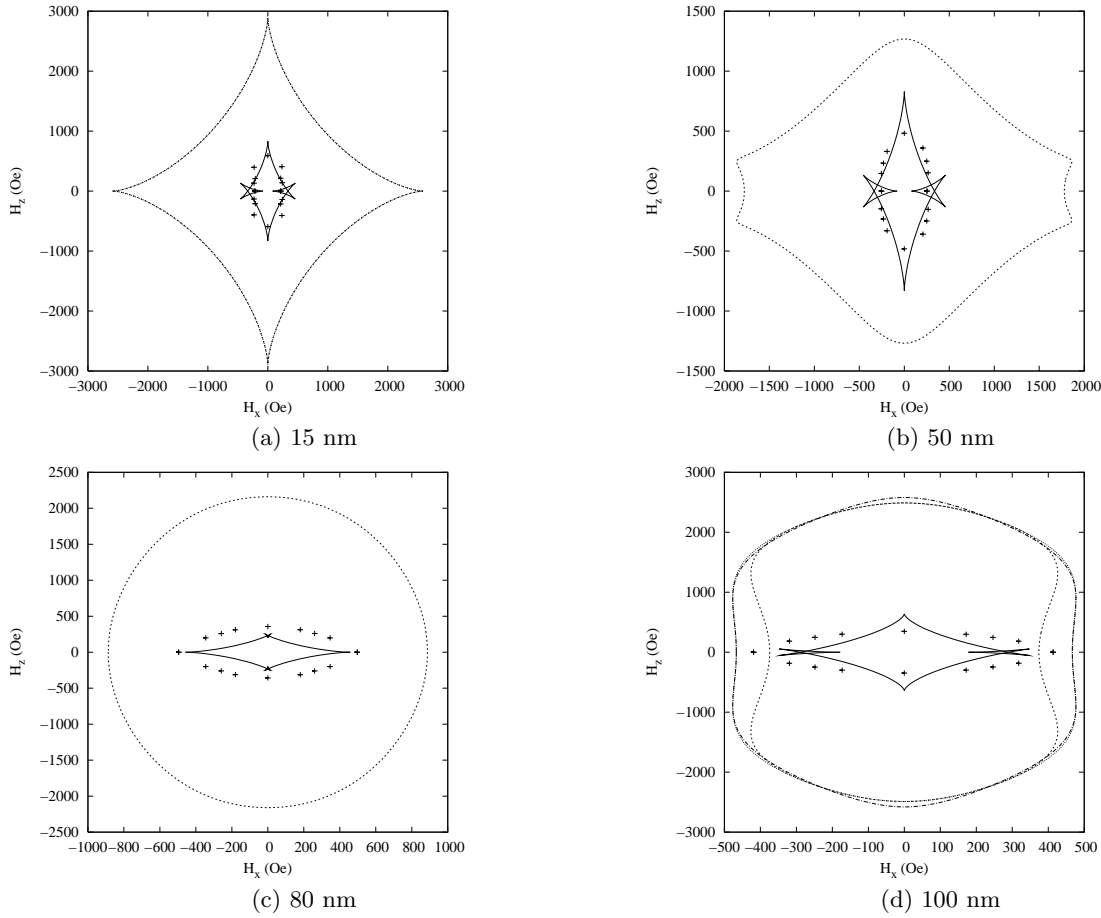


Fig. 6 – Comparison of least-squares fitting and measurements (+) on all Nickel nanowires in the cubic anisotropy case [15]. Geometric signature for the Ni nanowire experimental results with four sets of diameters: 15, 50, 80 and 100 nm. The fitting values are respectively: $M_s=195$ emu/cm³, $K_1=-223420$ erg/cm³ and $K_2=73198$ erg/cm³ for 15 and 50 nm and $M_s=56$ emu/cm³, $K_1=6035$ erg/cm³ and $K_2=-7255$ erg/cm³ for 80 and 100 nm diameters. The reduced radius is $S=0.728, 2.427, 3.883$ and 4.854 respectively. The framing curves are obtained from the fitted K_1, K_2 and the bulk value of M_s .

Discussion and Conclusion. – In conclusion, by means of theoretical studies and experimental measurements, we have investigated the reversal processes in ferromagnetic nanowires. Our systematic studies of the effect of the nanowire radius show that the magnetization reversal mechanism is strongly influenced by its value. Two rotation modes are considered as the most important: coherent rotation and curling. Good agreement between the measured magnetic properties of Ni nanowires and the theoretical calculations is obtained. However, further experimental work remains to be done in order to observe this transition.

APPENDIX. – The establishment of the geometric representation is based on the following steps:

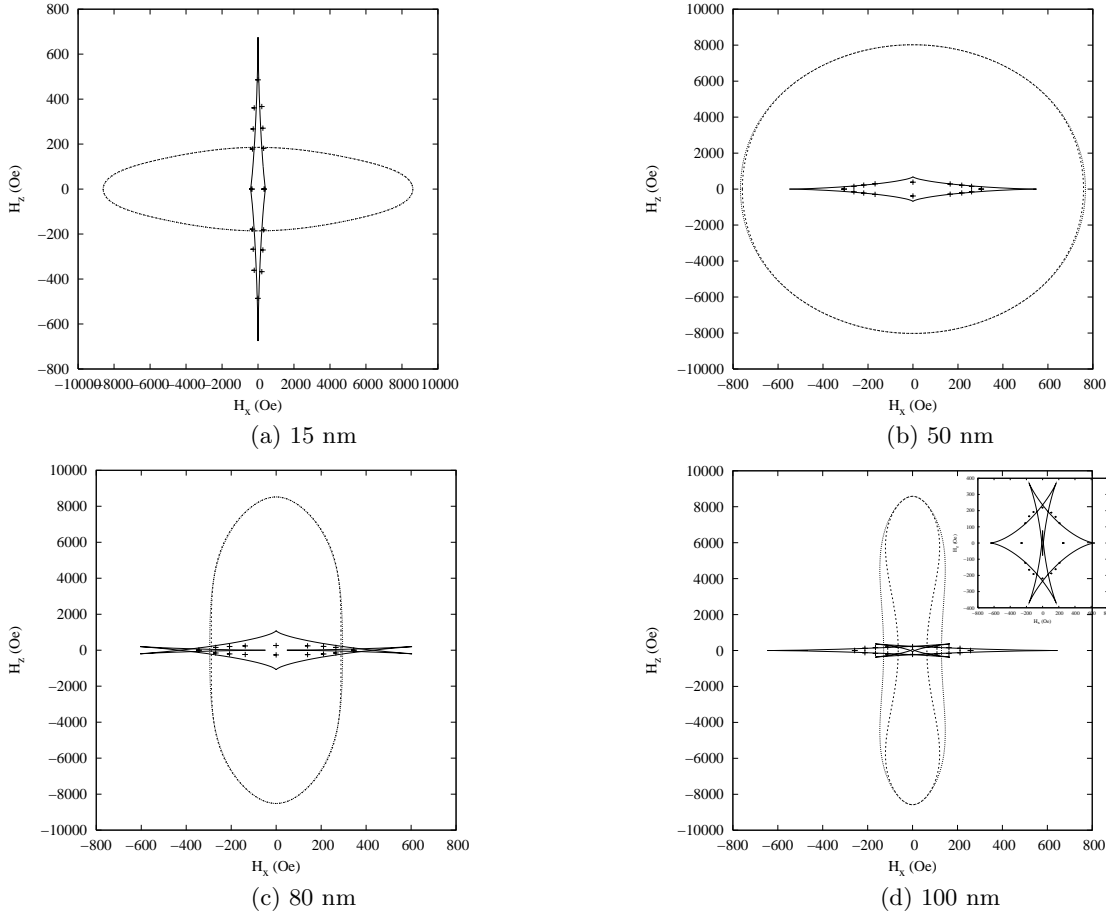


Fig. 7 – Comparison of least-squares fitting and measurements (+) on all Cobalt nanowires. Geometric signature for the Co nanowire experimental results with four sets of diameters: 15, 50, 80 and 100 nm. The fitting values are: $M_s = 87 \text{ emu/cm}^3$, $K_1 = -11333 \text{ erg/cm}^3$ and $K_2 = 11318 \text{ erg/cm}^3$ for 15 nm, $M_s = 105 \text{ emu/cm}^3$, $K_1 = -11691 \text{ erg/cm}^3$ and $K_2 = 7268 \text{ erg/cm}^3$ for 50 nm, $M_s = 44 \text{ emu/cm}^3$, $K_1 = -9912 \text{ erg/cm}^3$ and $K_2 = 22826 \text{ erg/cm}^3$ for 80 nm, and $M_s = 79 \text{ emu/cm}^3$, $K_1 = -90674 \text{ erg/cm}^3$ and $K_2 = 28643 \text{ erg/cm}^3$ for 100 nm diameter. The reduced radius is $S = 0.065, 0.262, 0.175$ and 0.396 respectively. The inset in the 100 nm case shows the detailed quality of the fit. The framing curves are obtained from the fitted K_1 , K_2 and the bulk value of M_s .

1. The equilibrium magnetization in the uniform case is first established. This entails writing the energy as $E = E_K + E_m + E_H$ where E_K is the anisotropy energy, E_m the magnetostatic (demagnetization) energy and E_H the Zeeman energy. The derivative $\frac{\partial E}{\partial \theta} = 0$ gives the equilibrium uniform magnetization \mathbf{M}_0 from the energy minimization.
2. The perturbation of the equilibrium (uniform) magnetization \mathbf{M}_0 by a non-uniform variation $\epsilon \mathbf{m}(\mathbf{r})$ leads to the space dependent total magnetization $\mathbf{M}(\mathbf{r}) = \mathbf{M}_0 + \epsilon \mathbf{m}(\mathbf{r})$ (see fig. 1) with the condition of local orthogonality $\epsilon \mathbf{m}(\mathbf{r}) \cdot \mathbf{M}_0 = 0$. From the non-uniform magnetization, $\mathbf{M}(\mathbf{r})$ one calculates the average value of the energy $E =$

$E_K + E_m + E_H + E_X$ over the nanowire where one explicitly introduces the exchange energy E_X stemming from non-uniformity. The total energy is now an even function of ϵ from symmetry consideration and is written as: $E(\theta, \epsilon^2)$. The minimization of $E(\theta, \epsilon^2)$ with respect to the perturbing amplitude ϵ^2 i.e. $\frac{\partial E}{\partial \epsilon^2} = 0$ gives the second set of equations that leads to the sought parametric representation.

For an Infinite cylinder, Shtrikman and Treves [18] were the first to derive the solution of the non-uniform magnetization in the $(\mathbf{u}, \mathbf{w}, \mathbf{y})$ system (see fig. 1) as given by:

$$\begin{aligned} \epsilon m_u &= -J_1(\lambda_n x) \frac{\sin \phi}{\cos \theta}, \\ \epsilon m_w &= J_1(\lambda_n x) \cos \phi, \end{aligned} \quad (12)$$

with λ_n the positive roots of the equation $\frac{dJ_1(x)}{dx} = 0$. The first solution ($n = 1$), that is the first positive maximum of $J_1(x)$ is $\lambda_1 = 1.841$ (see for instance Abramowitz and Stegun [10]). From the series representation of the Bessel function $J_1(\lambda x)$:

$$J_1(\lambda x) = \frac{\lambda x}{2} - \frac{(\lambda x)^3}{16} \dots \quad (13)$$

we get:

$$J_1(\lambda_1 x) = \frac{1.841}{2} x - \frac{(1.841)^3}{16} x^3 \dots \quad (14)$$

hence the Ishii [13] approximation for the $J_1(\lambda_1 x)$ function:

$$J_1(\lambda_1 x) \sim x - \frac{1}{3} x^3 \dots \quad (15)$$

that he used to evaluate the average energy over the cylinder.

The magnetization components to be considered are \widetilde{M}_i which are in the rotated frame $(\mathbf{u}, \mathbf{w}, \mathbf{y})$ (see fig. 1) with \mathbf{u} along the equilibrium magnetization \mathbf{M}_0 . The magnetostatic energy $2\pi N_{ij} \widetilde{M}_i \widetilde{M}_j$, $i, j = 1, 2, 3$ averaged over the volume of an infinite cylinder of radius a is given approximately by the average of $2\pi N_{ij} \widetilde{M}_i(r) \widetilde{M}_j(r)$ [19]. This means taking the demagnetization coefficients of the full cylinder and letting the magnetization $\widetilde{\mathbf{M}}(\mathbf{r})$ carry the spatial dependence. The averaging in the $(\mathbf{u}, \mathbf{w}, \mathbf{y})$ system yields:

$$\begin{aligned} \overline{E_m} &= \frac{1}{\pi a^2} \int_0^{2\pi} \int_0^a M_s^2 (1 + \alpha^2) \sin^2 \theta \, r dr d\varphi \\ &= \frac{M_s^2}{4\pi} \sin^2 \theta \left[1 - \frac{11}{72} \epsilon^2 \left(1 + \frac{1}{\cos^2 \theta} \right) \right] \end{aligned} \quad (16)$$

The average exchange energy is given by:

$$\begin{aligned} \overline{E_X} &= \frac{1}{\pi a^2} \int_0^{2\pi} \int_0^a A \left[(\nabla \widetilde{M}_x)^2 + (\nabla \widetilde{M}_y)^2 + (\nabla \widetilde{M}_z)^2 \right] r dr d\varphi \\ &= \frac{M_s^2}{4\pi} \epsilon^2 \frac{14}{27S^2} \left(1 + \frac{1}{\cos^2 \theta} \right) \end{aligned} \quad (17)$$

The average anisotropy and Zeeman energies are evaluated likewise such that:

$$\begin{aligned}\overline{E_K} &= K \left[\sin^2 \theta + \epsilon^2 \frac{11}{72} \left(\frac{\cos 2\theta}{\cos^2 \theta} + \cos^2 \theta \right) \right] \\ \overline{E_H} &= -M_s H \left[\cos(\theta - \phi) - \epsilon^2 \frac{11}{144} \left(1 + \frac{1}{\cos^2 \theta} \right) \cos(\theta - \phi) \right]\end{aligned}\quad (18)$$

REFERENCES

- [1] Z. Z. Sun and J. Schliemann, Phys. Rev. Lett. **104**, 037206 (2010).
- [2] M. Yan, A. Kakay, S. Gliga and R. Hertel, Phys. Rev. Lett. **104**, 057201 (2010).
- [3] C. T. Boone, J. A. Katine, M. Carey, J. R. Childress, X. Cheng, and I. N. Krivorotov, Phys. Rev. Lett. **104**, 097203 (2010).
- [4] N. D. Mermin and H. Wagner, Phys. Rev. Lett. **17**, 1133 (1966).
- [5] E.C. Stoner and E.P. Wohlfarth, Phil. Tran. Roy. Soc. Lond., **A240**, 599 (1948).
- [6] W.F. Brown Jr., *Micromagnetics*, Wiley Interscience Publishers, New-York (1963).
- [7] E.H. Frei, S. Shtrikman, and D. Treves, Phys. Rev. **106**, 446 (1957).
- [8] C. Kittel, *Introduction to Solid State Physics*, 7th edition, Wiley, New-York, p.460 (1996).
- [9] A. Aharoni, J. Appl. Phys. **82**, 1281 (1997).
- [10] M. Abramowitz and I.A Stegun, *Handbook of Mathematical Functions*, Table 9.5, p.411, Dover, New-York (1972).
- [11] A. Aharoni IEEE Trans. Mag. **34**, 2175 (1998).
- [12] S-K Chung and M. W. Muller, IEEE Trans. Mag. **24**, 340 (1972).
- [13] Y. Ishii, J. App. Phys. **70**, 3765 (1991).
- [14] The exchange length $\ell_{ex} = \sqrt{A/K}$ with A , the exchange stiffness constant ($A \sim 10^{-6}$ erg/cm) is obtained from the comparison between the exchange energy density (erg/cm³) $\frac{A_{ij}}{M_s^2} \frac{\partial M_k}{\partial x_i} \frac{\partial M_k}{\partial x_j} \sim \frac{A}{\ell_{ex}^2}$ and the anisotropy energy density $\frac{K_{ij}}{M_s^2} \mathbf{M}_i \mathbf{M}_j \sim K$ with K representing the (second-order) anisotropy constant of the material. In soft materials whose anisotropy constant $K \sim 0$, one uses the magnetostatic exchange length defined as $\ell_{ex} = \sqrt{A/2\pi M_s^2}$ since $K \sim 0$ in soft materials and the magnetostatic energy density is $2\pi M_s^2$.
- [15] Fourth-order uniaxial anisotropy energy is expressed as: $K_1 \sin^2 \theta + K_2 \sin^4 \theta$, whereas sixth-order cubic anisotropy energy is: $K_1(\alpha_1^2 \alpha_2^2 + \alpha_2^2 \alpha_3^2 + \alpha_3^2 \alpha_1^2) + K_2 \alpha_1^2 \alpha_2^2 \alpha_3^2$ where: $\alpha_1, \alpha_2, \alpha_3$ are the cosines of the angles that the magnetization makes with the $(\mathbf{x}, \mathbf{y}, \mathbf{z})$ axes respectively (see Fig. 1).
- [16] M. W. Muller and R. M. Goldstein J. App. Phys. **40**, 2459 (1969).
- [17] J-E Wegrowe, D. Kelly, A. Franck, S.E. Gilbert and J-Ph. Ansermet Phys. Rev. Lett. **82**, 3681 (1999).
- [18] S. Shtrikman, and D. Treves, J. Physique **20**, 286 (1959).
- [19] E. I. Kondorsky IEEE Trans. Mag. **15**, 1209 (1979).

